A Kinetics Model for Interphase Formation in Thermosetting Matrix Composites

F. Yang, R. Pitchumani

Composites Processing Laboratory, Department of Mechanical Engineering, University of Connecticut, Storrs, Connecticut 06269-3139

Received 19 July 2002; accepted 15 November 2002

ABSTRACT: During the cure of thermosetting polymer composites, the presence of reinforcing fibers significantly alters the resin composition in the vicinity of the fiber surface via several microscale processes, forming an interphase region with different chemical and physical properties from the bulk resin. The interphase composition is an important parameter that determines the micromechanical properties of the composite. Interphase development during processing is a result of the mass-transport processes of adsorption, desorption, and diffusion near the fiber surface, which are accompanied by simultaneous cure reactions between the resin components. Due to complexities of the molecular-level mechanisms near the fiber surface, few studies have been carried out on the prediction of the interphase evolution as function of the process parameters. To address this void, a kinetics model was developed in this study to describe the coupled mass-transfer and reaction processes leading to interphase formation. The parameters of the model were determined for an aluminum fiber/diglycidyl ether of bisphenol-A/bis(*p*-aminocyclohexyl)methane resin system from available experimental data in the literature. Parametric studies are presented to show the effects of different governing mechanisms on the formation of the interphase region for a general fiber–resin system. The interphase structure obtained from the model may be used as input data for the prediction of the overall composite properties.
 J Appl Polym Sci 89: 3220–3236, 2003

Key words: adsorption; composites; curing of polymers; interfaces; kinetics (polym.)

INTRODUCTION

Fabrication of thermosetting matrix composites is based on a critical step of cure, which involves applying a predefined temperature cycle to a fiber–resin matrix mixture. The elevated temperatures initiate a crosslinking cure reaction among the species in the matrix. The presence of fibers has been found to significantly influence the cure reaction, resulting in the formation of a third phase, known as the *interphase*, which possesses properties distinct from those of the bulk fiber and the matrix. The interphase resides in a region between the original constituents of the composite with a size of a few to a few thousand nanometers.[1–4] Although the region has a submicroscopic scale, it essentially forms a significant portion of the matrix in the composite.[1] Also, the performance of the composite is determined by the ability of the matrix to transfer load to the reinforcing fiber and is thus controlled by the interphase region. The structure and properties of the interphase are the dominant factors governing the overall composite properties and performance.

Prediction of the overall composite properties in the presence of the interphase region involves the following steps:[1]

- First, the manufacturing parameters must be linked with the interphase structures. For example, given a cure temperature and pressure cycle, the chemical composition of the interphase should be determined. In this step, physical and chemical mechanisms must be identified and modeled to predict the interphase structure.
- In the second step, the known interphase structure is related to the interphase material properties such as glass-transition temperature (T_g), flexural modulus, or thermal expansion coefficient. This step is primarily based on the experimental correlation of the interphase chemical composition to the measured interphase material properties.
- The last step is to link the interphase material properties to overall composite properties such as the strength, fracture, and environmental resistance.

A majority of the studies in the literature focus on the experimental determination of the influence of

Correspondence to: R. Pitchumani (r.pitchumani@uconn.edu).

Contract grant sponsor: National Science Foundation; contract grant number: CTS-9912093.

Contract grant sponsor: Air Force Office of Scientific Research; contract grant number: F496200110521.

interphase layers on the behavior of composite materials,[2–5] that is, steps 2 and 3. Surface treatment and sizing parameters are widely varied to tailor the structure of the interphase region and to examine the effects of different interphases on the mechanical behavior of the composite materials. Several studies have been conducted in this regard with experimental approaches or numerical calculations such as finite element methods.[4,6,7] The studies so far have provided insights into the qualitative description of the interphase regions and their influence on the composite properties for typical material systems used in practice.

The first step, that is, the prediction of the interphase structure as a function of the process parameters, forms the basis of the other two steps. However, due to complexities of the molecular-level mechanisms that occur in the vicinity of the fibers during the process, few investigations have been conducted in this area. The overhead comes from the fact that a dozen physical and chemical mechanisms contribute simultaneously to the formation of the interphase region, and only few of these mechanisms can be rigorously described in mathematical models. Garton et al.[8] showed that the carbon surfaces influenced the crosslinking reaction in an anhydride–epoxy system by adsorbing the tertiary amine catalyst and forming amine-rich interphase regions near the carbon surfaces. Similarly, Sellitti et al.[9] used Fourier transform IR attenuated total reflection spectroscopy to characterize the interphase phenomena in an epoxy–anhydride–catalyst system and showed that the surface species introduced on graphitized carbon fibers could promote or inhibit the crosslinking process by the preferential adsorption of the catalyst. Other possible interphase mechanisms were proposed by Drzal,[4] including: the skin area of the fiber might have morphological deviation from the bulk fiber; the surface proximity of the fiber changes the structure of the resin in the interphase; surface treatments give rise to chemically and structurally different regions near the fiber surface; exposure to air before composite processing results in the adsorption of impurities that are desorbed at elevated temperatures; and the presence of a thin monomer coating on the surface of the fiber.

To our knowledge, the first work on modeling interphase formation in thermosetting composites was presented by Palmese.[1] The model predicts the interphase composition under thermodynamic equilibrium conditions of an epoxy–amine resin mixture near a fiber surface. The Gibbs phase rule was used to set up the equilibrium state, accounting for the enthalpy interaction between fiber surface and resin components, and the calculation of Gibbs free energy was based on a Flory–Huggins type lattice structure. The model does not take the chemical reactions into account, and furthermore, because of the assumption of thermodynamic equilibrium, it cannot predict the interphase evolution with time during processing. Hrivnak[10] extended Palmese's model to a reacting system by using renewal theory models to construct the assembly Gibbs free energy and the associated chemical potential.

Adsorption from a mixture of polymer chains and solvent molecules near a surface was presented by Scheutjens and Fleer[11] with a statistical approach. The partition function for the mixture was evaluated with a quasicrystalline lattice model, which in turn, gave the number of chains in each conformation in equilibrium. The focus of the work was on polymer adsorption, whereas the interphase formation in thermosetting materials is based on monomer transport.

The objective of this study was to develop a kinetics model for the prediction of the interphase growth with time during thermosetting composite processing, which would account for the simultaneous cure reaction. The model describes the mass transfer of the monomer components in the composite system before the formation of the polymer macromolecules. Clearly, our intention was not to study all of the previously-mentioned mechanisms contributing to interphase development. Rather, our focus was on the mechanism of preferential adsorption of the resin components. The model development and analysis presented here were based on the rationale that for a given specific surface treatment and coating process, among others, the formation of the interphase is governed by manufacturing-process-dependent mechanisms, principally those of preferential adsorption. A systematic study of the adsorption mechanism will provide information on how the interphase evolves during the manufacturing processes and, in turn, point out ways to design cure cycles to optimally tailor the interphase.

Experimental studies[12–14] have shown that the adsorption of an epoxy system can form an interphase layer 100–500 nm in thickness, which indicates that adsorption effects penetrate beyond one molecular layer. In this study, a multilayer coupled adsorption–desorption–diffusion–reaction model was developed to predict the interphase composition evolution for a thermosetting system. The formulation was based on the principle of mass conservation applied to a domain consisting of discrete molecular layers. The model was correlated to experimental data reported in the literature to determine the parameters of the model. Parametric studies are presented to illustrate the effects of the various dimensionless parameters on the interphase development.

INTERPHASE FORMATION MODEL

The cure of thermosetting resin systems is characterized by the reaction between prepolymer (or mono-

mer) molecules and a curing agent to form a crosslinked network that cannot flow on vitrification. The reinforcing fibers alter the cure characteristics by selective adsorption of resin components, which changes the concentration of the reacting species in the vicinity of the fiber surfaces. The goal of this study was to predict the concentration profiles of the constituent species near the fiber surface by consideration of the processes that occur in the cure reaction. An inorganic fiber/epoxy–amine thermosetting system is considered in the following discussion; however, all of the derivations and results are applicable to a general two-component thermosetting system.

The geometry considered is the half-infinite space contacting an infinitely large flat fiber surface, which may be justified by the fact that the interphase thickness is much smaller in comparison to the fiber diameter. The fiber is considered to have an epoxy sizing layer applied to its surface. The sized fiber is exposed to an epoxy–amine resin mixture, and the epoxy and amine species begin reacting with each other at $t = 0^+$. Accompanying the chemical reaction, epoxy molecules diffuse away from the sizing layer adjacent to the fiber. In a reverse movement, the amine molecules diffuse into the sizing layer due to the relatively higher amine concentration in the bulk resin region. The diffusion process has a tendency to eliminate the concentration gradients. In addition, the "force field" of the fiber surfaces causes the epoxy and amine molecules to migrate in the direction towards the surfaces, a process referred to as adsorption. Also the adsorbed molecules may be desorbed to the bulk resin in a desorption process. Unlike the diffusion process, the net effect of the adsorption and desorption processes is the build up of concentration gradients. All the processes mentioned above take place simultaneously, resulting in a continuously evolving concentration profile that is "frozen" in space upon gelation of the thermosetting system.

The adsorption phenomenon at the equilibrium state near solid surfaces was described by Brunauer, Emmett, and Teller (referred to as the BET theory).[15,16] In this development, the concepts in BET theory were extended to the transient processes in the interphase evolution. Following the approach of the BET theory, the domain surrounding the fiber surface was divided into molecular layers where one molecule of epoxy or amine could occupy only one of these layers. Due to the interaction between resin molecules and the fiber surface, as well as those among resin molecules themselves, epoxy and amine molecules can move from layer to layer. Adsorption is a process where molecules bind in one or more layers onto a solid surface through chemical or physical forces. The molecules that bind to the surface are called the adsorbate[16] and are referred to be in the "adsorbed" state. Other molecules that are unbound to the surface are considered to be in the "bulk" state. The solid surface can adsorb molecules from a bulk state into an adsorbed state, and conversely, molecules in the adsorbed state may be desorbed into the bulk state. Molecules in the adsorbed state are treated to be fixed in the space and are not permitted to diffuse, whereas molecules in the bulk state may diffuse within the resin mixture.

Figure 1 shows the molecular layers in the model domain, where the adsorption layers contain molecules in the adsorbed state, whereas the bulk layers hold molecules in the bulk state. Although the adsorption and bulk layers are drawn separately to illustrate the mass exchange between the adsorbed and bulk states, the corresponding layers essentially occupy the same space; that is, the ith adsorption layer and the ith bulk layer overlap. The multiple adsorption layers are formed as follows: at $t = 0$, there are no molecules in the adsorbed layers because the adsorption process has not begun, and all of the resin molecules are in the bulk state. At the beginning of the process, $t = 0^+$, some bulk-state molecules in the first or second molecular layers are adsorbed into the first layer of the adsorbed state and occupy the adsorption sites on the bare fiber surface. Note that the molecules beyond the second layer cannot be adsorbed directly into the first layer because of the fact that they are out of contact with the first layer. In the next time step, three mass movements could happen: (1) some of the molecules adsorbed in the first layer could be desorbed into the bulk in the first and second layers, (2) the molecules in the bulk state in the first and second layers could be continuously adsorbed into the first layer at the remaining adsorption sites on the fiber surface, and (3) the molecules in the bulk state in the first, second, and third layers could be adsorbed on top of the molecules in the first adsorption layer, forming a second adsorption layer. Similar processes continue and result in a multilayer adsorbed state, as shown in Figure 1.

Because the molecules in the adsorbed state are not free to diffuse, the diffusion process is only driven by the concentration gradient in the bulk state. Chemical reactions between epoxy (E) and amine (A) happen simultaneously during the adsorption, desorption, and diffusion processes. The reaction equation may be written as

$$n_1\mathrm{E} + n_2\mathrm{A} \rightarrow \mathrm{P} \tag{1}$$

where P denotes the product and n_1 and n_2 are the molar numbers of the reactants needed to produce 1 mol of product.

The governing equations for the mechanisms discussed so far may be derived with the principle of mass conservation for a control volume (CV); namely, the rate of increase of mass in the CV (storage) equals the difference between the rate of mass flow into the CV and the total depletion of mass from the CV aris-

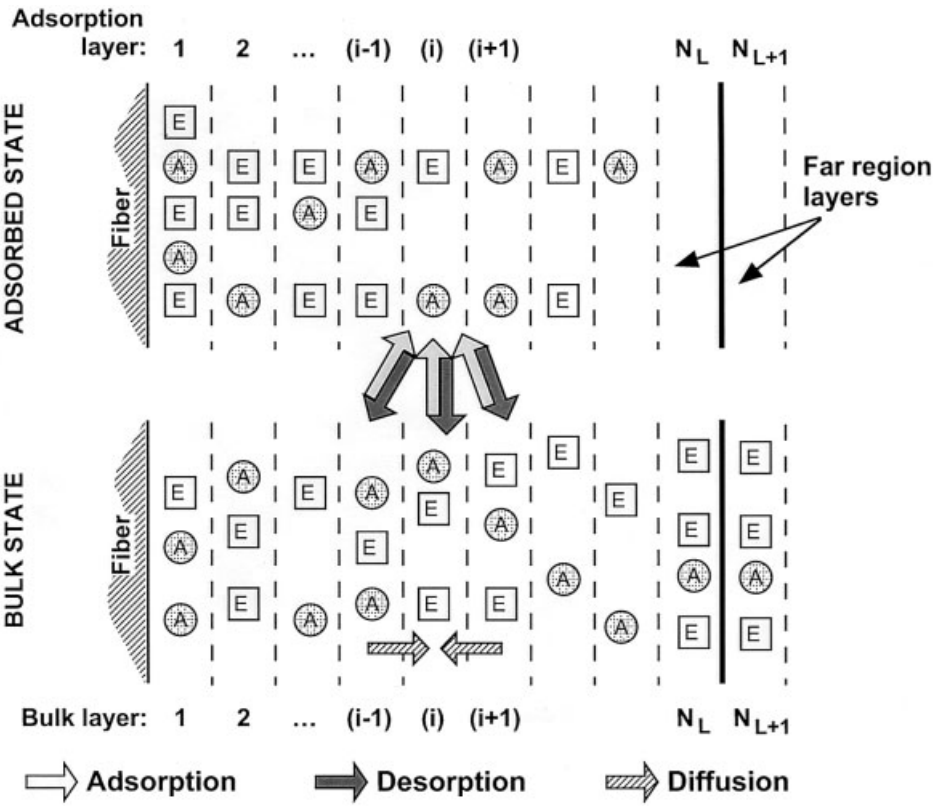

Figure 1 Schematic of the adsorption, desorption, and diffusion processes in an epoxy-amine system.

ing from mass outflow and mass consumption due to chemical reactions. With any ith adsorption layer in Figure 1 referred to as a CV, the principle of mass conservation for the epoxy molecule yields

$$\underbrace{\frac{dN_{E,i}}{dt}}_{\text{Storage}} = \underbrace{R_{a,E}(i-1,\,i) + R_{a,E}(i,\,i) + R_{a,E}(i+1,\,i)}_{\text{Adsorption, } \Re_{a,E}(i)}$$

$$\underbrace{- R_{d,E}(i-1,\,i) - R_{d,E}(i,\,i) - R_{d,E}(i+1,\,i)}_{\text{Desorption, } \Re_{d,E}(i)}$$

$$\underbrace{- \Re_{r,E}(i)}_{\text{Depletion (reaction)}} \tag{2}$$

where $dN_{E,i}/dt$ is the rate of change of the total number of epoxy molecules in the ith adsorption layer, and the subscripts E and i denote the epoxy and ith layer, respectively. Epoxy molecules in the bulk state in the $(i-1)$th, ith, and $(i+1)$th layers may be adsorbed into the ith molecular layer, denoted by the rate terms $R_{a,E}(i-1,\,i)$, $R_{a,E}(i,\,i)$, and $R_{a,E}(i+1,\,i)$, respectively; in a reverse process, the adsorbed epoxy molecules in the ith layer can be desorbed into the bulk in the $(i-1)$th, ith, and $(i+1)$th layers, and their respective rates are denoted as $R_{d,E}(i-1,\,i)$, $R_{d,E}(i,\,i)$, and $R_{d,E}(i+1,\,i)$. Further, the depletion of epoxy in the ith adsorption layer through chemical reaction is represented by the rate term $\Re_{r,E}(i)$.

The determination of the rate terms of adsorption, desorption, and reaction are illustrated in the following discussion. The adsorption of epoxy molecules from the $(i-1)$th layer of the bulk state to ith layer of the adsorbed state is given as

$$R_{a,E}(i-1,\,i) = k_{a,E}(N_{i-1} - N_i) \times \exp\left(-\frac{E_{a,E}}{RT}\right)\frac{N_{E\infty,i-1}}{N_{\infty,i-1} + N_{\infty,i} + N_{\infty,i+1}} \tag{3}$$

where the parameter $k_{a,E}$ is the frequency factor in the adsorption rate of epoxy molecules and N_i is the total number of epoxy and amine molecules adsorbed in the ith layer, that is, $N_i = N_{E,i} + N_{A,i}$. Because a molecule adsorbed into the ith layer must adjoin an adsorbed epoxy or amine molecule in the $(i-1)$th layer, the term $N_{i-1} - N_i$ yields the number of available sites in the $(i-1)$th layer that are open for adsorption. For $i = 1$, the term $N_0 - N_1$ denotes the available sites in the first adsorption layer, where N_0 is the number of adsorption sites on the bare fiber surface. The activation energy of adsorption for the epoxy molecules is denoted as $E_{a,E}$, which defines the energy barrier to be crossed for an epoxy molecule to be adsorbed, and R and T in Eq. (3) are the Universal gas constant and the temperature, respectively. The pa-

rameters $N_{E\infty,i}$ and $N_{A\infty,i}$ are the number of epoxy and amine molecules in the bulk state in the ith molecular layer, and $N_{\infty,i} = N_{E\infty,i} + N_{A\infty,i}$. Because the epoxy molecules adsorbed into the ith layer come from the $(i - 1)$th, ith, and $(i + 1)$th layers, the fraction $(N_{E\infty,i-1}/N_{\infty,i-1} + N_{\infty,i} + N_{\infty,i+1})$ in eq. (3) denotes the probability that a site can capture an epoxy molecule from the $(i - 1)$th layer of the bulk state. It is intuitively expected that the parameter $k_{a,E}$ should vary from layer to layer, corresponding to a progressively decreasing adsorption force field away from the fiber surface. However, because the variation of $k_{a,E}$ is not readily obtained from existing theoretical or experimental means, the adsorption rate, $k_{a,E}$, and all other adsorption/desorption rates are assumed to be independent of location, as in the BET theory. This assumption will be relaxed in the future development of the model.

Other rate terms can be defined in a similar way, and are summarized next:

$$R_{a,E}(i, i) = k_{a,E}(N_{i-1} - N_i) \times exp\left(-\frac{E_{a,E}}{RT}\right)\frac{N_{E\infty,i}}{N_{\infty,i-1} + N_{\infty,i} + N_{\infty,i+1}} \quad (4)$$

$$R_{a,E}(i + 1, i) = k_{a,E}(N_{i-1} - N_i) \times exp\left(-\frac{E_{a,E}}{RT}\right)\frac{N_{E\infty,i+1}}{N_{\infty,i-1} + N_{\infty,i} + N_{\infty,i+1}} \quad (5)$$

$$R_{d,E}(i - 1, i) = R_{d,E}(i, i) = R_{d,E}(i + 1, i) = \frac{1}{3}k_{d,E}(N_i - N_{i+1})\exp\left(-\frac{E_{d,E}}{RT}\right)\frac{N_{E,i}}{N_i} \quad (6)$$

$$\Re_{r,E}(i) = n_1 k_r N_{E,i} \quad (7)$$

where $R_{d,E}(i - 1, i)$ is the rate term of the desorption of epoxy molecules from the ith absorption layer to the $(i - 1)$th bulk layer, $R_{d,E}(i, i)$ is the rate term of the desorption of epoxy molecules from the ith absorption layer to the ith bulk layer, and $R_{d,E}(i + 1, i)$ is the rate term of the desorption of epoxy molecules from the ith absorption layer to the $(i + 1)$th bulk layer. The fraction $\frac{1}{3}$ in the desorption terms arises from the assumption that the probabilities of desorption from the ith adsorbed layer to each of the three neighborhood bulk layers are identical. The parameter $k_{d,E}$ is the frequency factor in the desorption rate of epoxy molecules. Because a molecule in the adsorbed layer i can be desorbed into the bulk state only if the molecule has no molecule adjoining it in the $(i + 1)$th adsorbed layer, the term $N_i - N_{i+1}$ yields the number of molecules in the ith adsorbed layer that may be desorbed into the bulk state. The activation energy of desorption $(E_{d,E})$ for the epoxy molecules defines the energy barrier to be crossed for an epoxy molecule to be desorbed. The fraction $N_{E,i}/N_i$ arises from the fact that among all of the molecules desorbed from the ith adsorbed layer, the probability of finding an epoxy molecule is its molar fraction in the adsorbed layer. The depletion term, $\Re_{r,E}(i)$ in eq. (2), is determined by the crosslinking chemical reaction between epoxy and amine, where k_r is the reaction rate.

A similar mass conservation analysis may be applied to the amine molecules in the adsorbed state and to the product molecules, yielding the following equations for these species:

$$\underbrace{\frac{dN_{A,i}}{dt}}_{\text{Storage}} = \underbrace{R_{a,A}(i - 1, i) + R_{a,A}(i, i) + R_{a,A}(i + 1, i)}_{\text{Adsorption, } \Re_{a,A}(i)} - \underbrace{R_{d,A}(i - 1, i) - R_{d,A}(i, i) - R_{d,A}(i + 1, i)}_{\text{Desorption, } \Re_{d,A}(i)} - \underbrace{\Re_{r,A}(i)}_{\text{Depletion (reaction)}} \quad (8)$$

$$\frac{dN_{P,i}}{dt} = k_r N_{E,i} \quad (9)$$

where the rate terms are defined similarly to those in eqs. (3)–(7) by changing the subscript E (epoxy) to A (amine), and $\Re_{r,A}(i)$ is the rate term representing the depletion of amine in the ith absorption layer through chemical reaction. The right hand side of eq. (9) has only the reaction term because the product molecules are assumed to have no mobility and will stay in their space of formation. Also, $N_{P,i}$ is the number of product segments in the ith layer due to the reaction in the adsorbed state.

Equations (2), (8), and (9) pertain to the mass transfer rates of the molecules in the adsorbed state. The adsorbed state exchanges mass with the bulk state, in which the molecules undergo diffusion in addition to the adsorption, desorption, and reaction processes. Considering the rate of change of the number of epoxy molecules in the bulk state in the ith layer, that is, $dN_{E\infty,i}/dt$, the following four types of contributions were identified: (1) diffusion of epoxy molecules in the bulk state from the $(i + 1)$th and $(i - 1)$th layers to ith layer, which increases $N_{E\infty,i}$; (2) desorption of epoxy molecules in the adsorbed state in the $(i - 1)$th, ith, and $(i + 1)$th layers to the ith layer of the bulk state, which increases $N_{E\infty,i}$; (3) epoxy molecules in the bulk state in the ith layer being adsorbed to the $(i - 1)$th, ith, and $(i + 1)$th layers of the adsorbed state, which reduces

$N_{E\infty,i}$; and (4) chemical reaction in the bulk in ith layer, which depletes $N_{E\infty,i}$. We then obtained

$$\frac{dN_{E\infty,i}}{dt} = D_{EA}\left(\frac{N_{E\infty,i-1} + N_{E\infty,i+1} - 2N_{E\infty,i}}{\Delta L^2}\right) + R_{d,E}(i, i-1) + R_{d,E}(i, i) + R_{d,E}(i, i+1) - R_{a,E}(i, i-1) - R_{a,E}(i, i) - R_{a,E}(i, i+1) - n_1 k_r N_{E\infty,i} \quad (10)$$

where D_{EA} is the mutual diffusion coefficient in the binary epoxy–amine mixture and ΔL corresponds to the physical size of a molecular layer. All the rate terms were defined previously [eqs. (3)–(6)]. Similarly, we obtained the rate equations for $N_{A\infty,i}$ and $N_{P\infty,i}$ as

$$\frac{dN_{A\infty,i}}{dt} = D_{EA}\left(\frac{N_{A\infty,i-1} + N_{A\infty,i+1} - 2N_{A\infty,i}}{\Delta L^2}\right) + R_{d,A}(i, i-1) + R_{d,A}(i, i) + R_{d,A}(i, i+1) - R_{a,A}(i, i-1) - R_{a,A}(i, i) - R_{a,A}(i, i+1) - n_2 k_r N_{E\infty,i} \quad (11)$$

$$\frac{dN_{P\infty,i}}{dt} = k_r N_{E\infty,i} \quad (12)$$

where $N_{P\infty,i}$ is the number of product segments in the ith layer due to the reaction in the bulk state.

The rate equations for species in the bulk state must be solved simultaneously with those corresponding to the adsorbed state. The diffusivity (D_{EA}) and k_r are functions of the extent of cure. The diffusivity is described by free-volume theory as[17]

$$D_{EA} = D_0 \exp(-E_D/RT)\exp[-b_D/(f_g + \alpha_f[T - T_g(\xi)])] \quad (13)$$

where D_0, f_g, and α_f are constants; E_D is the activation energy; and b_D is an empirical constant. $T_g(\xi)$ defines the available free volume and degree of rotational restriction, which in turn, are functions of the reaction extent, $\xi = N_E(t)/N_{E0}$, defined as the ratio of the total concentration of epoxy at a time instant to that at time zero (initial concentration). The parameters D_0, b_D, f_g, α_f, and E_D in the model depend on the type of thermosetting system and can be determined by the approach described by Sanford.[17] The DiBenedetto equation relates T_g to the extent of cure as[17]

$$\frac{T_g(\xi) - T_g^0}{T_g^0} = \frac{(E_x/E_m - F_x/F_m)(1 - \xi)}{1 - (1 - F_x/F_m)(1 - \xi)} \quad (14)$$

where the constants T_g^0, E_x/E_m, and F_x/F_m can be obtained through experimental data of T_g versus ξ. k_r is controlled by the retarded diffusion process at later stages of the cure and is given as

$$k_r = \frac{k_{r0}\exp(-E_a/RT)}{1 + \frac{\delta_0}{D_{EA}}\exp(-E_a/RT)} \quad (15)$$

where k_{r0} is the Arrhenius pre-exponential constant, δ_0 is the coordination sphere reaction parameter, and E_a is the reaction rate activation energy.[17]

The unknowns in eqs. (2)–(12) are the number of molecules, $N_{E,i}$, $N_{A,i}$, $N_{P,i}$, $N_{E\infty,i}$, $N_{A\infty,i}$, and $N_{P\infty,i}$. When i goes from 1 (corresponding to the layer adjacent to the fiber surface) to N_L (corresponding to a far region layer), we have six more unknown variables than equations because the equations for N_Lth layer involve the number of molecules in the (N_L + 1)th layer. We assumed that the influence of the fiber surface cannot propagate to an infinite distance, which yielded two conditions for the far region: (1) the numbers of molecules in the adsorbed state are zero, and (2) the numbers of molecules in the bulk state are constants. The far region conditions provide six additional equations:

$$[\text{Adsorbed state}]\ N_{E,N_L+1} = 0; \quad N_{A,N_L+1} = 0; \quad N_{P,N_L+1} = 0$$
$$[\text{Bulk state}]\ N_{E\infty,N_L} = N_{E\infty,N_L+1}; \quad N_{A\infty,N_L} = N_{A\infty,N_L+1}; \quad N_{P\infty,N_L} = N_{P\infty,N_L+1} \quad (16)$$

Equations (2) and (8)–(12), where $i = 1, 2, \ldots, N_L$, and the far region conditions constitute a complete ordinary differential equation system for the $6N_L$ unknowns. For a thermosetting system with a fiber sizing thickness of N_S molecular layers, the initial conditions of the ODE system are (1) the numbers of molecules for each species in the adsorbed state and the number of product in the bulk state are zero; (2) within the epoxy sizing layer, the number of the epoxy is a constant, $N_{E,1}$, whereas the number of the amine is zero; and (3) beyond the sizing layer, the numbers of epoxy and amine species are constants, $N_{E,0}$ and $N_{A,0}$, respectively. The mathematical expressions for the initial conditions may be written as:

$$N_{E,i} = N_{A,i} = N_{P,i} = N_{P\infty,i} = 0 \quad (i = 1, 2, \ldots, N_L)$$
$$N_{E\infty,i} = N_{E,1}; \quad N_{A\infty,i} = 0 \quad (i = 1, 2, \ldots, N_S)$$
$$N_{E\infty,i} = N_{E,0}; \quad N_{A\infty,i} = N_{A,0} \quad (i = N_S + 1, \ldots, N_L) \quad (17)$$

The initial conditions for the species in the adsorbed state require that the resin mixture is separated from

TABLE I
Properties of the DGEBA/PACM20 Resin Components[14]

Resin component	M (g/mol)	ρ (kg/m^3)
DGEBA	382.4	1170
PACM20	198.3	960

the fiber surface before $t \leq 0$, which corresponds to the manufacturing processes of the thermosetting prepregs or processes such as resin transfer molding. For composite materials processing that utilizes prepregs, the initial conditions may be changed to the concentration profiles within the prepreg materials.

Equations (2) and (8)–(12) were solved with a fourth-order Runge–Kutta method.[18] Corresponding to the numerical range of the dimensionless groups introduced later in this article, a dimensionless time step of 0.001 yielded converged results. The numerical computations were carried out until the system reached its gelation point, which was defined as the point where the total number of the epoxy molecules reduced to 40% of its original value.

RESULTS AND DISCUSSION

The model developed in the previous section was used to calculate the molar concentration of the resin components as a function of molecular layers under isothermal conditions, $T = T_0$, where T_0 is the constant temperature at which the process takes place. The model was correlated to the concentration profile measured experimentally by Arayasantiparb et al.[14] to determine the parameters of the model. The experimental study measured the composition of an epoxy–aluminum interphase with spatially resolved electron energy-loss spectroscopy (EELS) in a scanning transmission electron microscope. The material system consisted of an aliphatic bis(*p*-aminocyclohexyl)methane (PACM20) curing agent, an aromatic diglycidyl ether of bisphenol-A (DGEBA) epoxy resin, and a single aluminum fiber with a diameter of 125 μm. The properties of the resin components as reported in ref. 14 are given in Table I. Energy-loss spectra were collected for the DGEBA/PACM20 system at different locations of the sample and were used to determine the local volume fraction of PACM20. More discussion on the experimental measurement can be found in ref. 14.

Because the experimental data was presented in the form of PACM20 (in a binary mixture of DGEBA and PACM20) volume fraction as a function of distance from the aluminum fiber surface, the molar numbers and molecular layer used in the model needed to be transformed to the corresponding quantities. The physical dimensions of the molecular layers in the system could be estimated as the size of resin molecules. The calculations assumed the molecules to be spheres and a uniform molecular weight distribution equal to the average molecular weight. The assumptions could be relaxed if we accounted for a monomer molecular weight and shape distribution to arrive at better estimates of the sizes. The molecular volume v_m was found as $v_m = (M/\rho N_a)$, where M, ρ, and N_a are the molecular weight, density, and Avogadro's number, respectively. The size of each molecular layer was estimated as $[6v_m/\pi]^{1/3}$ and was evaluated to be 1.00 nm from the size of the DGEBA molecules. The size of PACM20 molecules was 0.87 nm, which was similar to that of DGEBA. Furthermore, the molar concentrations of each species could be transformed to volume fractions through the expression $n = (V\rho/M)$, where n is the molar number of a species and V is the volume. The volume fraction of PACM20 (Φ_A) may be related to its molar fraction (X_A) as

$$\Phi_A = \frac{X_A M_A/\rho_A}{X_A M_A/\rho_A + (1 - X_A)M_E/\rho_E}$$

where the subscripts, E and A, denote the DGEBA and PACM20, respectively.

The goal of the correlation study was primarily to examine the ability of the model to reflect the physical trends in the data. At this stage, a systematic approach to directly determine all the parameters of the model is not available and may be a subject of future work. An optimization program implementing the simulated annealing method[19] was used to minimize the objective function that defines the sum of the squares of the difference between the model prediction of the composition profile and the experimental data from Arayasantiparb et al.[14] The objective function is governed by eight independent variables, namely, the diffusion parameters, $D_0\exp(-E_D/RT)/\Delta L^2$ and b_D; the reaction parameter, $k_{r0}\exp(-E_a/RT)$; the relative number of adsorption sites on the fiber surface, N_0/N_{E0}; and the adsorption and desorption rate parameters, $k_{a,E}\exp(-E_{a,E}/RT)$, $k_{d,E}\exp(-E_{d,E}/RT)$, $k_{a,A}\exp(-E_{a,A}/RT)$, and $k_{d,A}\exp(-E_{d,A}/RT)$ where $k_{a,A}$ is the absorption rate of amine molecules, $E_{a,A}$ is the adsorption activation energy of amine molecules, $k_{d,A}$ is the desorption rate of amine molecules, and $E_{d,A}$ is the desorption activation energy of amine molecules. The method of simulated annealing draws analogy from thermodynamics, specifically the way that liquids freeze and crystallize or that metals cool and anneal. At high temperatures, molecules move freely with respect to one another. If the cooling is carried out slowly, the atoms often line themselves up probabilistically and form a pure, ordered crystalline structure, which represents a minimum energy state. Analogously, the optimization objective function is treated as an energy, and for an assumed cooling schedule, called the annealing schedule, the design configurations undergo a series of

TABLE II
Model Parameters Reported in the Literature for the DGEBA/PACM20 System[17]

Parameter	Value	Parameter	Value
E_x/E_m	0.337	F_x/F_m	0.194
T_g^0 (K)	254	f_g	0.025
α_f (K^{-1})	5.0×10^{-4} ($T > T_g$); 5.0×10^{-5} ($T < T_g$	δ_0 (cm^2/s)	0.220

probabilistic rearrangements, eventually leading to the minimum energy solution. More detail is available in the literature on the optimization technique.[19]

The parameters of the model available in the literature[17] are given in Table II, and the values of the parameters obtained from the correlation are tabulated in Table III. The following observations are illustrated in Table III: (1) the adsorption rate of DGEBA, $k_{a,E}\exp(-E_{a,E}/RT)$, was three orders of magnitude smaller than its desorption rate, $k_{d,E}\exp(-E_{d,E}/RT)$, indicating that the aluminum surface did not have affinity with the DGEBA molecules; (2) the adsorption rate of PACM20, $k_{a,A}\exp(-E_{a,A}/RT)$, was two orders of magnitude larger than its desorption rate, $k_{d,A}\exp(-E_{d,A}/RT)$, denoting a preferential adsorption on the PACM20 species as reported by Arayasantiparb et al.; (3) the value of reaction rate, $k_{r0}\exp(-E_a/RT)$, was similar to that reported by Sanford,[17] and (4) the value of diffusivity determined by the parameters $D_0\exp(-E_D/RT)/\Delta L^2$ and b_D was roughly an order of magnitude larger than that reported by Sanford, and (5) the number of adsorption sites on the aluminum surface (N_0) was about 65% of the initial number of DGEBA molecules in the bulk (N_{E0}). In most cases, the fitting results were consistent with the data in the literature.

Figure 2(a) shows the correlation results in terms of the PACM20 volume fraction as a function of distance from the aluminum wire surface. The dashed line denotes the experimental data, and the solid line corresponds to model prediction. The prediction closely followed the data over the entire range. The concentration of PACM20 in terms of percentage volume was a large value, 80%, at the aluminum surface, indicating a preferential adsorption on the species, and decreased sharply away from the fiber surface. In the region between 100 and 1500 nm, experimental measurements were not reported, and Arayasantiparb et al.[14] stated that the concentration was a constant bulk value of 25%. As shown in Figure 2(a), the model predicted a decrease in the concentration to 22% before the recovery of the bulk concentration at 25%. The model prediction pointed to the fact that the mass aggregation in the region 0–100 nm had to be compensated by the mass deficit beyond the region. However, the deficit may be too small to have been discerned in the experimental measurement technique. Figure 2(b) shows a close-up view of Figure 2(a) in the region 0–100 nm. The error bars of the experimental data as provided in ref. 14 are included for comparison. Overall, Figure 2 demonstrates the ability of the model to represent the physical trends. As pointed out previously, the parameters of the model should be

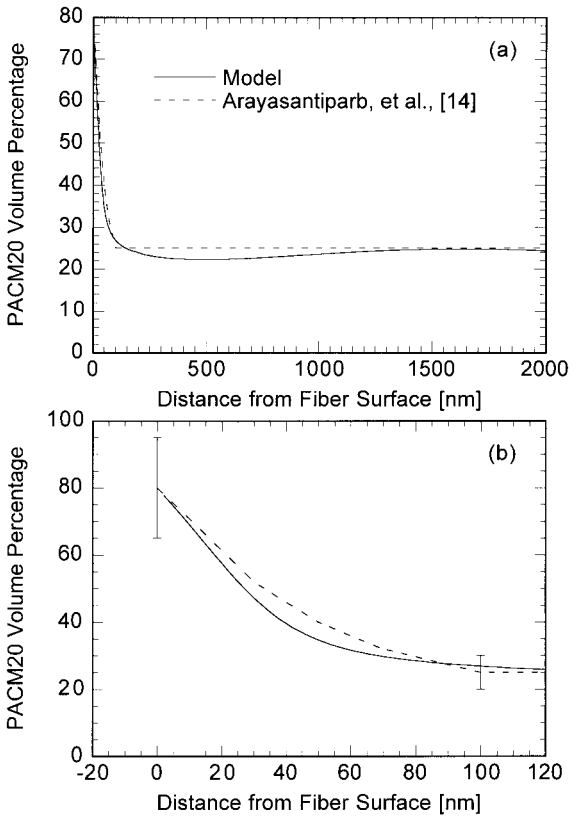

Figure 2 Comparison of the interphase composition profile predicted by the model and available experimental data[14] for an aluminum fiber/DGEBA-PACM20 system, over (a) a relative large region from the fiber surface, and (b) the interphase region.

TABLE III
Model Parameters Determined by the Correlation to Experimental Data

Parameter	Value	Parameter	Value
$D_0\exp(-E_D/RT)/\Delta L^2$ (1/s)	6.05×10^4	b_D	5.48×10^{-2}
$k_{r0}\exp(-E_a/RT)$ (1/s)	1.08×10^{-4}	N_0/N_{E0}	0.65
$k_{aE}\exp(-E_{aE}/RT)$ (1/s)	2.04×10^{-5}	$k_{dE}\exp(-E_{dE}/RT)$ (1/s)	1.58×10^{-2}
$k_{aA}\exp(-E_{aA}/RT)$ (1/s)	0.85	$k_{dA}\exp(-E_{dA}/RT)$ (1/s)	1.03×10^{-2}

determined through direct experimental or theoretical methods in a future work.

With the correlation results of the interphase formation model as basis, parametric studies were conducted to illustrate the effects of different parameters on the interphase composition and thickness of an epoxy/amine system. Dimensionless forms of eqs. (2)–(12) were used to identify relevant nondimensional groups that governed the process. By introducing a dimensionless time (t') as $k_{a,E}e^{-(E_{a,E}/RT_0)}t$ and dividing all the number of molecules (e.g., $N_{E,i}$, $N_{A,i}$, N_0) by the initial number of epoxy molecules in the far region layers (N_{E0}; e.g., $N'_{E,i} = N_{E,i}/N_{E0}$), we identified the principal dimensionless groups as follows: (1) epoxy desorption ratio, $\beta_E = (k_{d,E}/k_{a,E})e^{-(E_{d,E}-E_{a,E})/RT_0}$; (2) amine desorption ratio, $\beta_A = (k_{d,A}/k_{a,E})e^{-(E_{d,A}-E_{a,E})/RT_0}$; (3) amine adsorption ratio, $\alpha_A = (k_{a,A}/k_{a,E})e^{-(E_{a,A}-E_{a,E})/RT_0}$; (4) adsorption Damköhler number, $\gamma = (k_r/k_{a,E})e^{(E_{a,E}/RT_0)}$; and (5) diffusion ratio, $\phi_{EA} = (D_{EA}/\Delta L^2 k_{a,E})e^{(E_{a,E}/RT_0)}$. In the parametric study, the number of molecular layers in the model domain was kept fixed at $N_L = 100$, and the physical dimension of a molecular layer was chosen to be 1.00 nm, that is, the value for the DGEBA/PACM20 system.

Figures 3–5 present the evolution of the concentration profiles with time for three selected scenarios to illustrate the influence of each mechanism considered in the model. Although the total concentrations are the most relevant to the composite material properties, the results of the adsorbed and bulk fractions are presented as well to better elucidate the trends in the total concentration development. Figure 3(a–f) shows the distributions of the number of epoxy and amine molecules from the fiber surface (layer 1) to the far region (layer 100) at different nondimensional times during the process. Figure 3(a,b) presents the concentration profiles for the molecules in the adsorbed state, Figure 3(c,d) corresponds to bulk state concentration profiles, and Figure 3(e,f) shows the total concentrations of epoxy and amine, $N'_{E,\mathrm{tot}}$ and $N'_{A,\mathrm{tot}}$, respectively. The results correspond to the parameter combination of $N_S = 0$ (i.e., without a sizing layer), $\gamma = 0$, $\beta_E = 0.5$, $\alpha_A + 1.5$, $\beta_A = 0.5$, $N'_{E0} = N'_{A0} = 1$, $N'_{E,1} = 2$, $N'_0 = 1$ [$N'_0 = (N_0/N_{E0})$], and $\phi_{EA} = 60.0$. γ was set to zero to examine the effects of the adsorption and desorption processes in the absence of chemical reactions. The desorption ratios β_E and β_A were relatively small, which indicated that the resin molecules were easily adsorbed onto the fiber surface.

In the adsorbed state profiles, Figure 3(a,b), the number of molecules for both of the species increased due to adsorption onto the surface, resulting in a high concentration region near the fiber surface. The concentration profiles propagated from a small region near the fiber surface at $t' = 0.2$ to the far region at the final time $t' = 102.0$, which was identified as a strong adsorption effect. The number of epoxy molecules near the fiber surface was smaller than that of the amine molecules because of the larger amine adsorption rate ($\alpha_A = 1.5$). The adsorption/desorption processes caused the deficit of species in the bulk state near the fiber surface, as shown in Figure 3(c,d) from $t' = 0.2$ to $t' = 25.0$. However, the diffusion process compensated for the deficit at the final time, $t' = 102.0$, when the concentration gradients in the bulk state approached zero. The total concentration profiles of each species [Fig. 3(e,f)] showed minima at $t' = 10.0$ and $t' = 25.0$, which could be explained by the coupled influence of the adsorption/desorption and the diffusion processes as discussed.

The interphase thickness is a critical factor influencing the overall composite performance and properties, as noted in the literature.[3,7] For example, Rydin et al.[3] reported that a thin ductile interphase increased the interlaminar toughness through crack blunting, enhanced frictional sliding, and greater part deflections prior to fracture. However, a further increase in the thickness was shown to facilitate debonding and delamination because the strong adhesion between fiber and matrix was replaced by weak dipole–dipole interactions between the interphase and the matrix. In another study, Liu et al.[7] found that when the modulus of the interphase was greater than that of the matrix, an increase in the interphase thickness (δ) led to an increase in the overall composite modulus.

Interphase thickness may be defined in a similar way as the boundary layer thickness in fluid mechanics, such as the number of layers from the fiber surface beyond which the epoxy concentration is within 1% of the epoxy concentration in the far region layers [Fig. 3(e)]. A similar thickness, δ_A, may be defined on the basis of the amine concentration profile. With the thickness based on the epoxy concentration profile denoted as δ_E, an overall δ was determined in this study as the larger of the two values obtained from the epoxy and amine profiles, that is, $\delta = \max(\delta_E, \delta_A)$. As shown in Figure 3(e,f), the interphase was thin at an early time ($t' = 0.2$) and grew as the process progressed ($t' = 102.0$); the profiles at $t' = 102.0$ are the equilibrium profiles representing the balance among the adsorption, desorption, and diffusion processes. For the combination of parameters in Figure 3, because of the absence of the reaction and the relatively small desorption, the influence of the fiber surface propagated all the way to the far region layer, leading to a very thick or no distinct interphase formation at the final time.

Figure 4(a–f) presents the concentration profile evolution, following the presentation format in Figure 3(a–f), for the parameter combination of $\beta_E = 1.5$, $\alpha_A = 0.5$, and $\beta_A = 2.0$; all other parameters retained the values as in Figure 3. Figure 4(a,b) shows that the concentration profiles in the adsorbed state grew from $t' = 0.2$ to $t' = 10.0$ and remained invariant afterward.

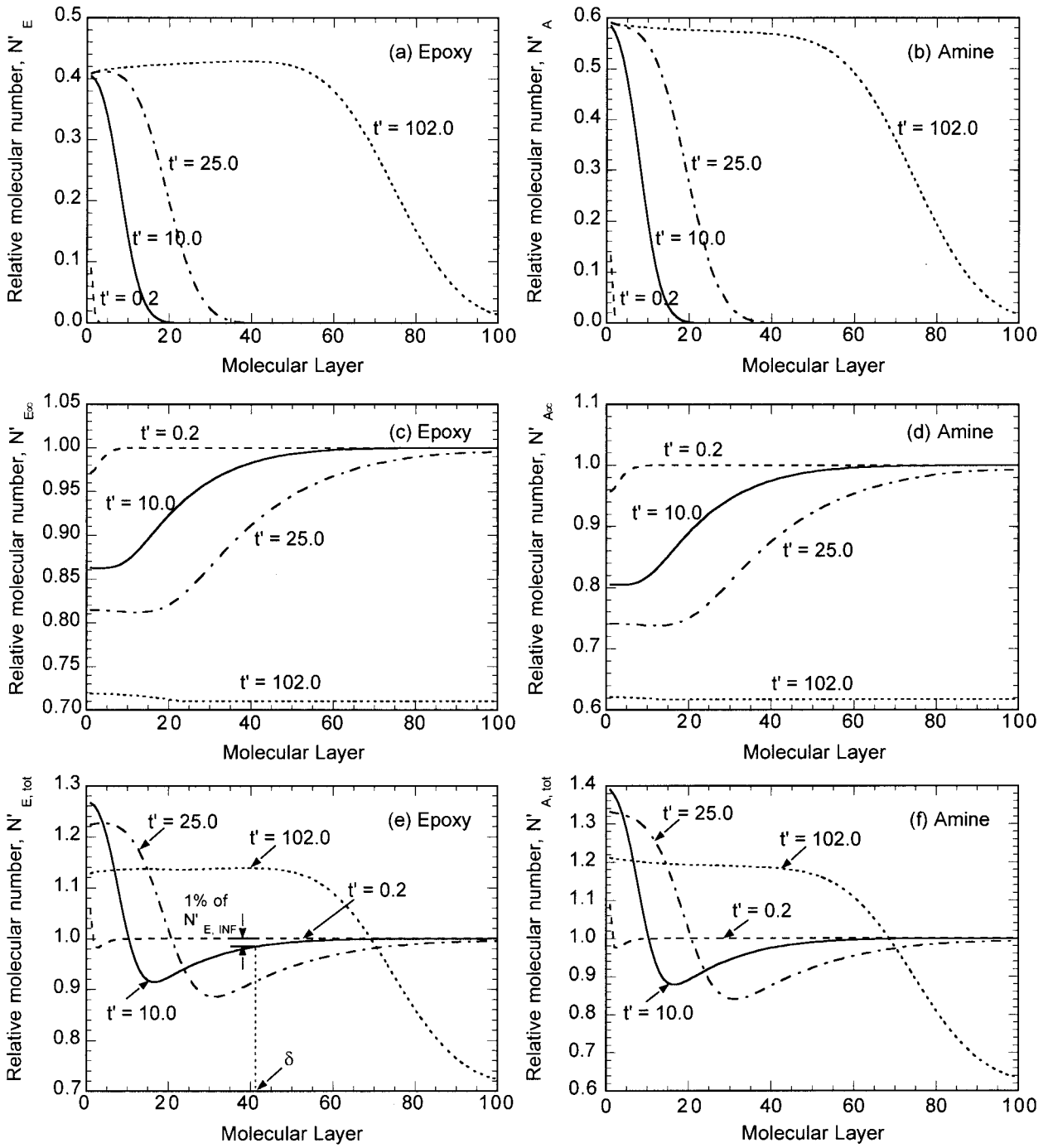

Figure 3 Interphase concentration profiles in terms of the relative number of (a) epoxy molecules in the adsorbed state, and (b) amine molecules in the adsorbed state; (c) epoxy molecules in the bulk state, and (d) amine molecules in the bulk state; (e) total epoxy molecules in both states, and (f) total amine molecules in both states, as a function of the molecular layer at four different times during the isothermal cure process. The parameter combination corresponds to a unsized system with strong adsorption effect and zero reaction rate.

An equilibrium state was thus reached, where the desorption and adsorption processes balanced each other and the influence of the fiber surface only propagated to a few molecular layers. The concentration profiles in the bulk state [Fig. 4(c,d)] predicted large concentration gradients at time $t' = 0.2$; at $t' > 0.2$, because to the diffusion process, the gradients decreased and reached zero at $t' = 82.0$. At $t' = 10.0$ and $t' = 25.0$, the regions with nonzero gradients in the bulk state were wider than the corresponding regions in the adsorbed state. Consequently, the total concentration profiles [Fig. 4(e,f)] showed that the interphase thickness first increased from $t' = 0.2$ to $t' = 25.0$, mostly due to the contributions from the bulk state,

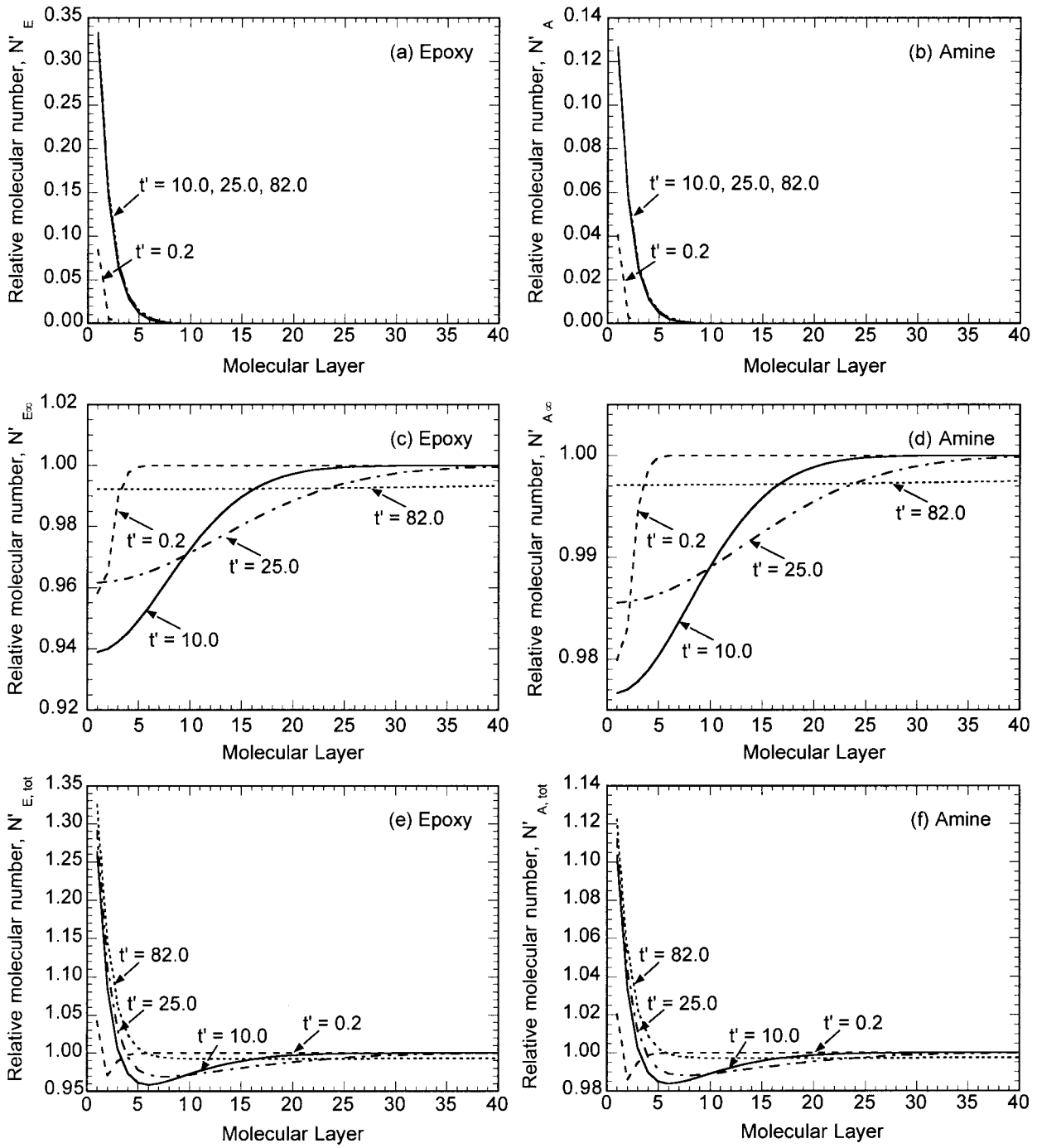

Figure 4 Interphase concentration profiles in terms of the relative number of (a) epoxy molecules in the adsorbed state, and (b) amine molecules in the adsorbed state; (c) epoxy molecules in the bulk state, and (d) amine molecules in the bulk state; (e) total epoxy molecules in both states, and (f) total amine molecules in both states, as a function of the molecular layer at four different times during the isothermal cure process. The parameter combination corresponds to a unsized system with weak adsorption effect and zero reaction rate.

and then decreased to a smaller value governed by the adsorbed state gradients at time $t' = 82.0$, when the diffusion gradients were zero. This scenario is in contrast to what is shown in Figure 3, where a strong force field by the fiber surface penetrated the entire resin domain. Through an increase in β_A and β_E and a decrease in α_A, the desorption process was strengthened with respect to adsorption, which corresponded to a relatively weak force field by the fiber surface that could only penetrate into a few molecular layers.

The parametric studies presented so far pertained to concentration evolution of a resin/fiber system without sizing layers on the fiber surface. The application of an epoxy sizing on the fiber surface is a common

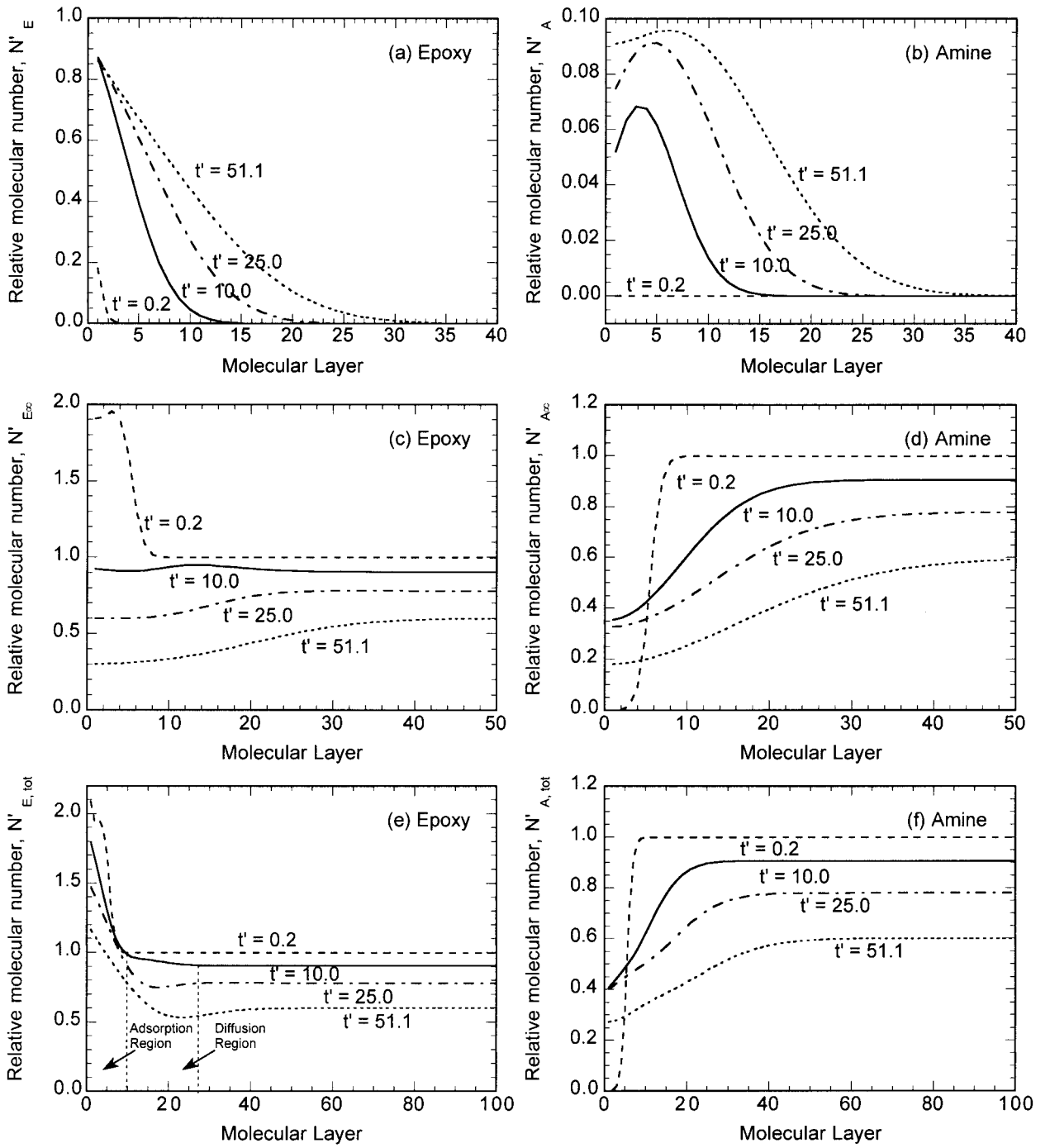

Figure 5 Interphase concentration profiles in terms of the relative number of (a) epoxy molecules in the adsorbed state, and (b) amine molecules in the adsorbed state; (c) epoxy molecules in the bulk state, and (d) amine molecules in the bulk state; (e) total epoxy molecules in both states, and (f) total amine molecules in both states, as a function of the molecular layer at four different times during the isothermal cure process. The parameter combination corresponds to a sized system with relative large reaction rate.

practice in the manufacturing process, and we were interested in examining its effect on the interphase evolution. Figure 5 follows the same presentation format as Figures 3 and 4 to show the concentration profiles evolution of a system with sizing. The result corresponds to the parameter combination of $N_S = 5$, $\gamma = 5.0$, $\beta_E = 0.5$, $\alpha_A = 1.5$, and $\beta_A = 0.5$, and all other parameters retained the same values as previously stated for Figure 3. Recall that the mass transfer through the adsorption, desorption, and diffusion processes is dramatically slowed when the reacting resin system reaches the gelation point, and the final concentration profiles can be approximated by the profiles at the gelation point. Because γ de-

termines the gelation time and, in turn, the available time for the mass transfer processes, as γ increases, the available time decreases. In Figure 5, γ is set to be relatively large, providing only a limited time for the mass transfer processes to develop.

The concentration of epoxy in the adsorbed state increased with time, and the growth was stopped by the reaction at the gelation time $t' = 51.1$, as shown in Figure 5(a). The amine concentration profiles, shown in Figure 5(b), had maxima near the fiber surface, which may be explained as follows: because the epoxy sizing directly contacted the fiber surface, epoxy molecules occupied most of the adsorption sites near the fiber surface, and most of the amine molecules could only be adsorbed on top of the epoxy molecules. Therefore, the amine concentration was small at the fiber surface, followed by an increase within a few molecular layers around the fiber due to adsorption and then a decrease as the net adsorption diminished in the region away from the fiber. As shown in Figure 5(c,d), the initially large concentration of epoxy and zero concentration of amine (at $t' = 0.2$) near the fiber surface correspond to the epoxy sizing layer applied on the fiber. At the gelation time ($t' = 51.1$), the concentration gradients in the bulk were small but greater than zero because the gelation time is not long enough for the diffusion process to reach equilibrium.

At time $t' = 10.0$, the total epoxy profile [Fig. 5(e)] had two distinct regions: a large gradient region near the fiber surface, followed by a small gradient region. An examination of the concentration profiles of the epoxy species in the adsorbed state [Fig. 5(a)] and bulk state [Fig. 5(c)] separately revealed that the large gradient region came from the profile in the adsorbed state, whereas the small gradient region was determined by the profile in the bulk state. These are shown in Figure 5(e) as the adsorption region and the diffusion region, respectively, for the particular time instant $t' = 10.0$. These regions grew away from the fiber with time, with the gradients in the diffusion region approaching zero because the tendency of the diffusion to equilibrate the concentration, whereas the gradient in the adsorption region approached an equilibrium value, corresponding to the net balance of the adsorption and desorption effects. Two minima of the epoxy concentration are shown in Figure 5(e), at $t' = 25.0$ and $t' = 51.1$, respectively, which can be explained by the fact that epoxy molecules were adsorbed onto the fiber surface from the neighborhood, resulting in the deficiency of the epoxy species, which was not sufficiently replenished through the diffusion process. Figure 5(f) presents the amine concentration evolution with time. In this case, the diffusion and adsorption mass transfer were in the same direction, toward the fiber surface, as opposed to that in Figure 5(e), where the adsorption caused epoxy migration toward the fiber, and diffusion tended to move the epoxy molecules away from the fiber.

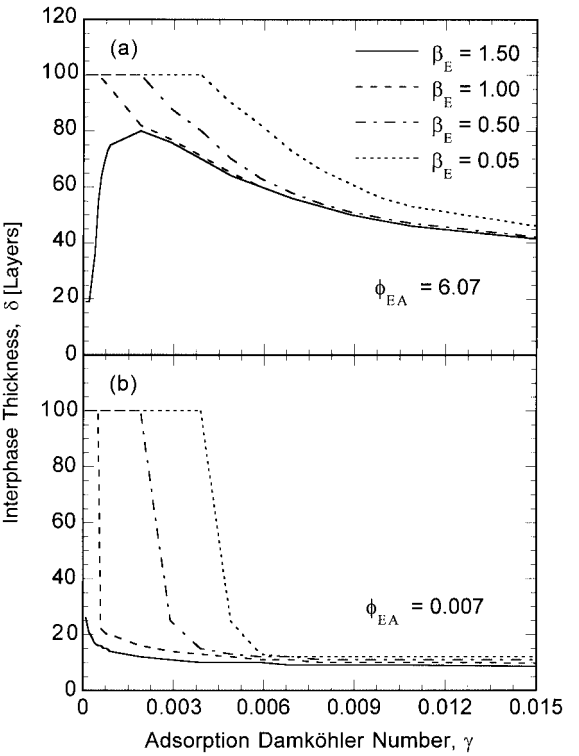

Figure 6 Interphase thickness as a function of adsorption Damköhler number, γ, at various epoxy desorption ratios, β_E, for (a) $\phi_{EA} = 6.07$ and (b) $\phi_{EA} = 0.007$.

An interphase thickness could be identified on the basis of the total concentration profiles, as shown in Figure 3(e). The interphase thickness is a concise representation of the interphase concentration profiles. As discussed previously, it critically influences the composite properties and constitutes an important input in the micromechanical models.[1,7] It is, therefore, instructive to examine the influence of each mechanism studied in the model on the interphase thickness. Figures 6–8 illustrate the roles of the various mechanisms involved and provide insight on the overall process. In Figure 6(a), the interphase thickness at the gelation time is plotted as a function of γ for different values of β_E. The result corresponded to the parameter combination of $\alpha_A = 1.0$, $\beta_A = 1.0$, $\phi_{EA} = 6.07$, and $N_S = 5$, and all of the other parameters retained their values as in Figure 3. In the parametric studies of the epoxy–amine system, the maximum thickness value was taken to be $N_L = 100$ layers. For the case of no reaction (i.e., $\gamma = 0$), which corresponded to an infinitely long interphase growth time, the diffusion process was fully developed, and the interphase concentration gradient and thickness were only determined by the net adsorption. For the case of $\beta_E = 0.05$, the small value indicated that the fiber surface had a strong net adsorption, which may have penetrated to

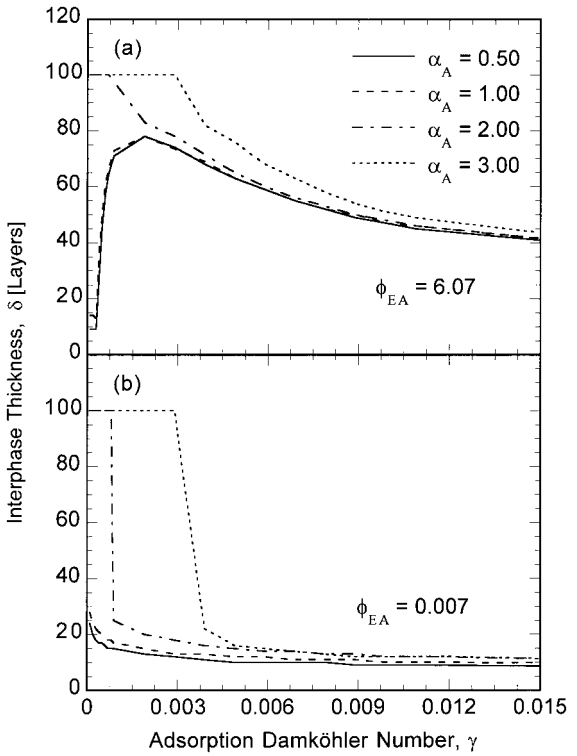

Figure 7 Interphase thickness as a function of adsorption Damköhler number, γ, at various amine adsorption ratios, α_A, for (a) $\phi_{EA} = 6.07$ and (b) $\phi_{EA} = 0.007$.

the entire resin domain given enough time. Therefore, when $\gamma = 0$, the curve started at the maximum thickness—100 layers. As γ increased, less time was available for the interphase development, and the thickness decreased monotonically. The same trend was observed for $\beta_E = 0.50$ and 1.00, which also had relatively strong net adsorptions.

With the increase in γ from zero, the increased reaction rate corresponded to less time available for the transport processes prior to gelation. The diffusion profile was, therefore, arrested before completion, which led to a thick diffusion. Because the adsorption/desorption concentration gradients were confined to a region near the fibers, the overall interphase thickness was governed by the diffusion profile, which led to an increased interphase thickness, as shown in Figure 6(a) for a β_E of 1.50. The increase in the interphase thickness from $\gamma = 0$ to a nonzero value was primarily due to the shift in the contribution to the interphase gradient from that of adsorption/desorption only (for $\gamma = 0$) to that of diffusion (for a small γ not equal to zero). With a further increase in the reaction rate (i.e., an increase in γ), the progressive decrease in the available time for the transport processes led to a monotonic decrease in the interphase thickness. In fact, as γ approaches infinity (the case of an infinitely fast reaction), the interphase composition should be that of the initial condition, and the interphase thickness should be the sizing thickness, N_S. As shown in the trend in Figure 6(a), all of the curves asymptotically approach this value (beyond the range of the plot). Furthermore, for a fixed γ, the interphase thickness decreased monotonically with increasing β_E because more molecules were desorbed from the interphase region.

Figure 6(b) has the same parameter combination as Figure 6(a) except that the diffusion ratio was set to $\phi_{EA} = 0.007$ to show the effect of sluggish diffusion. The interphase thicknesses predicted in Figure 6(b) reflect the negligible contribution of the diffusion process and were always smaller than or equal to the corresponding values shown in Figure 6(a). Also, for the weak net adsorption cases, Figure 6(b) did not exhibit the peaks shown in Figure 6(a), again due to the small diffusion.

Figure 7(a) presents the interphase thickness as a function of γ and α_A. The result corresponded to the parameter combination $\beta_A = 2.0$, $\beta_E = 1.0$, $\phi_{EA} = 6.07$, and $N_S = 5$, with all the other parameters retaining the same values as in Figure 3. The diffusion ratio ϕ_{EA} of 6.07 denoted a relatively active diffusion process. The parameter α_A reflected the relative attraction strength of the fiber surface to the epoxy and amine molecules, with $\alpha_A > 1$ denoting a preferential adsorption of the amine molecules. Through an increase in α_A, surface attraction to amine molecules was strengthened, which led to a thicker interphase rich in amine concentration. The influence of γ can be discussed by

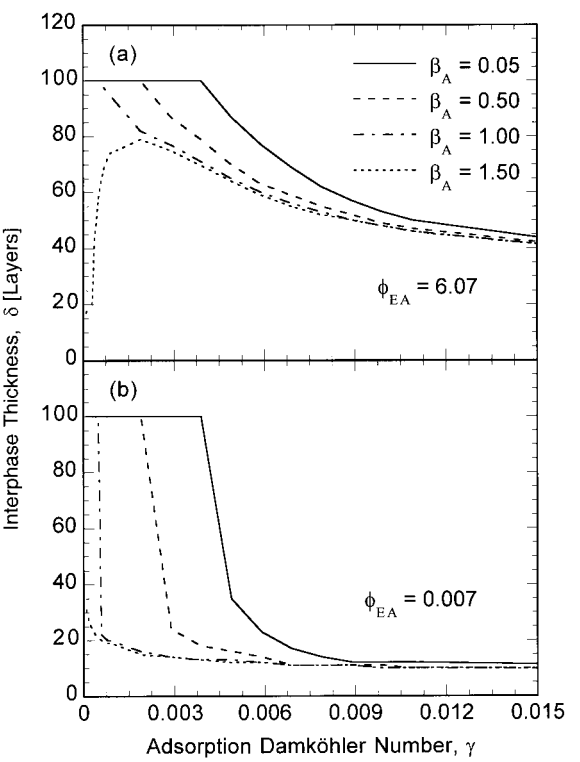

Figure 8 Interphase thickness as a function of adsorption Damköhler number, γ, at various amine desorption ratios, β_A, for (a) $\phi_{EA} = 6.07$ and (b) $\phi_{EA} = 0.007$.

similar considerations to those for the β_E effect in Figure 6. For strong net adsorption (corresponding to $\alpha_A = 2.0$ and 3.0), the thickness decreased monotonically from the maximum thickness of 100 layers with the increase of γ, whereas in the cases of weak net adsorption (corresponding to $\alpha_A = 0.5$ and 1.0), the thickness increased first due to the contribution of the diffusion and then decreased gradually. All the curves tended to the initial sizing thickness for $\gamma \to \infty$. At a constant value of γ, the interphase thickness increased monotonically with the increase in α_A because of the enhancement of the net adsorption.

Figure 7(b) represents the interphase thickness variation for the same parameter combination as in Figure 7(a) except for a ϕ_{EA} of 0.007 to illustrate the effect of weak diffusion. Similar to the discussion of Figure 6(b), the interphase thicknesses predicted in Figure 7(b) did not have a significant contribution of the diffusion process and were always smaller than or equal to the corresponding values shown in Figure 7(a). Again, for the weak net adsorption cases, Figure 7(b) does not exhibit the peaks shown in Figure 7(a) due to the lack of diffusion.

In Figure 8(a,b), the interphase thickness is presented as a function of γ and β_A. The result corresponded to the parameter combination of $\alpha_A = 1.0$, $\beta_E = 1.0$, $\phi_{EA} = 6.07$, and $N_S = 5$, with all the other parameters retaining the same values as in Figure 3. From eqs. (2) and (8), it follows that β_A had the same parametric effect as β_E, in that large values of β_A and β_E corresponded to weak net adsorption effects. Because the trends in Figure 8 were similar to those in Figure 6, the reader may examine to the corresponding discussion earlier. Although Figures 6 and 8 give similar thickness variations with corresponding desorption rates, the interphase compositions in the two cases were different; that is, a large β_E value corresponded to an epoxy-deficient interphase, whereas a large β_A value corresponded to an amine-deficient interphase. These two types of interphase would, therefore, lead to completely different properties of the overall composite.

The predicted interphase composition and thickness are important input data to the models that calculate the overall composite material properties. A significant step in a future work will be to determine the parameters involved in the kinetics model. Within the framework of the current model, the parameters may be evaluated by following the procedure outlined in the correlation study. In this case, the EELS measurements must be conducted systematically on the desired materials and temperatures to provide the concentration data in the interphase region. The current model is based on phenomenological descriptions of the kinetics of the governing transport processes without resorting to the calculations of the driving forces. Alternatively, the development of the thermodynamic or statistical models mentioned previously[1,10] involved detailed consideration of the driving forces (e.g., the enthalpy forces or entropy forces) and the complex motion and configuration of polymer molecules under these forces. The thermodynamic and kinetics approaches are equivalent if a relationship between the driving forces and the kinetics parameters can be established.

In this study, the temperature was taken as a given constant, whereas the real temperature field during a cure process needs to be solved by coupling to the energy equation for the whole composite domain. The cure cycles in the manufacturing processes act as boundary conditions for the energy equation to influence the temperature field, which in turn, controls the adsorption–desorption–diffusion–reaction processes and interphase formation. Therefore, through optimization of the cure cycle, the interphase can be tailored for a specific material system's requirements. These issues are presently under investigation to enhance the capabilities of the current model.

CONCLUSIONS

An adsorption–desorption–diffusion–reaction model was developed to predict the evolution of the interphase during isothermal cure of thermosetting resin systems. The parameters of the model were determined through a correlation to available experimental data on a DGEBA/PACM20 system. Parametric studies revealed that the concentration profiles showed minima or maxima instead of following simple monotonical patterns. In the case of strong net adsorption, as indicated by large values of adsorption rates and small values of desorption rates, the interphase thickness decreased monotonically with increasing reaction rate. Weak net adsorption resulted in peaks in the interphase thickness curves with respect to the reaction rate, due to the influence of the diffusion. A notable contribution of this study was the ability to predict the time evolution of the interphase. The predicted interphase composition and thickness may be used as input data for the finite element analysis of the overall composition properties, eliminating the need to assume input data values. The model may be combined with a macroscopic thermochemical model to establish the influence of the cure cycle on the interphase formation. This, in turn, will lead to the capability to tailor the interphase via optimal cure cycle selection.

NOMENCLATURE

b_D	empirical constant in the diffusion coefficient expression in eq. (13)
D_0	constant in the diffusion coefficient expression in eq. (13) (m^2/s)
D_{EA}	mutual diffusion coefficient in the binary epoxy–amine structure (m^2/s)

E_a activation energy in the reaction rate expression in eq. (15) (J/kg)
$E_{a,A}$ adsorption activation energy of amine molecules (J/kg)
$E_{a,E}$ adsorption activation energy of epoxy molecules (J/kg)
E_D activation energy in the diffusion coefficient expression in eq. (13) (J/kg)
$E_{d,A}$ desorption activation energy of amine molecules (J/kg)
$E_{d,E}$ desorption activation energy of epoxy molecules (J/kg)
E_x/E_m constant in the DiBenedetto expression in eq. (14)
f_g constant in the diffusion coefficient expression in eq. (13)
F_x/F_m constant in the DiBenedetto expression in eq. (14)
$k_{a,A}$ adsorption rate of amine molecules (s^{-1})
$k_{a,E}$ adsorption rate of epoxy molecules (s^{-1})
$k_{d,A}$ desorption rate of amine molecules (s^{-1})
$k_{d,E}$ desorption rate of epoxy molecules (s^{-1})
k_r reaction rate (s^{-1})
k_{r0} Arrhenius preexponential constant in the reaction rate expression in eq. (15) (s^{-1})
M molecular weight (kg/kmol)
M_A molecular weight of PACM20 (kg/kmol)
M_E molecular weight of DGEBA (kg/kmol)
n_1 number of moles of epoxy molecules (mol)
n_2 number of moles of amine molecules (mol)
N'_a Avogadro's number
N_0 number of adsorption sites available for adsorption on the fiber surface
N'_0 dimensionless variable ($N_0/N_{E,0}$)
N_i total number of adsorbed resin molecules in the ith layer
$N_{\infty,i}$ total number of resin molecules in the bulk state in the ith layer
$N_{A,0}$ initial number of amine molecules at the far region layers
$N_{A,i}$ number of adsorbed amine molecules in the ith layer
$N'_{A,i}$ dimensionless variable ($N_{A,i}/N_{E,0}$)
$N_{A\infty,i}$ number of amine molecules in the bulk state in ith layer
$N'_{A,\infty}$ dimensionless variable ($N_{A,\infty}/N_{E,0}$)
$N'_{A,\mathrm{tot}}$ total concentration of amine
$N_{E,0}$ initial number of epoxy molecules at the far region layers
$N_{E,1}$ initial number of epoxy molecules in the sizing layer
$N_{E,i}$ number of adsorbed epoxy molecules in the ith layer
$N'_{E,i}$ dimensionless variable ($N_{E,i}/N_{E,0}$)
$N_{E\infty,i}$ number of epoxy molecules in the bulk state in the ith layer
$N'_{E,\infty}$ dimensionless variable ($N_{E,\infty}/N_{E,0}$)
$N'_{E,\mathrm{tot}}$ total concentration of epoxy
N_L the number of the far region layer where all of the resin molecules are at the bulk state and where the composition becomes constant beyond this layer
$N_{P,i}$ number of product segments in the ith layer due to the reaction in the adsorbed state
$N'_{P,i}$ dimensionless variable ($N_{P,i}/N_{E,0}$)
$N_{P\infty,i}$ number of product segments in the ith layer due to the reaction in the bulk state
$N'_{P,\infty}$ dimensionless variable ($N_{P,\infty}/N_{E,0}$)
N_S number of sizing layers
R Universal gas constant (J/kg k)
$R_{a,A}(i-1, i)$ rate term of the adsorption of amine molecules from the $(i-1)$th bulk layer to the ith adsorption layer (s^{-1})
$R_{a,A}(i, i)$ rate term of the adsorption of amine molecules from the ith bulk layer to the ith adsorption layer (s^{-1})
$R_{a,A}(i+1, i)$ rate term of the adsorption of amine molecules from the $(i+1)$th bulk layer to the ith adsorption layer (s^{-1})
$R_{d,A}(i-1, i)$ rate term of the desorption of amine molecules from the ith adsorption layer to the $(i-1)$th bulk layer (s^{-1})
$R_{d,A}(i, i)$ rate term of the desorption of amine molecules from the ith adsorption layer to the ith bulk layer (s^{-1})
$R_{d,A}(i+1, i)$ rate term of the desorption of amine molecules from the ith adsorption layer to the $(i+1)$th bulk layer (s^{-1})
$R_{a,E}(i-1, i)$ rate term of the adsorption of epoxy molecules from the $(i-1)$th bulk layer to the ith adsorption layer (s^{-1})
$R_{a,E}(i, i)$ rate term of the adsorption of epoxy molecules from the ith bulk layer to the ith adsorption layer (s^{-1})
$R_{a,E}(i+1, i)$ rate term of the adsorption of epoxy molecules from the $(i+1)$th bulk layer to the ith adsorption layer (s^{-1})

$R_{d,E}(i-1, i)$ rate term of the desorption of epoxy molecules from the ith adsorption layer to the $(i-1)$th bulk layer (s^{-1})

$R_{d,E}(i, i)$ rate term of the desorption of epoxy molecules from the ith adsorption layer to the ith bulk layer (s^{-1})

$R_{d,E}(i+1, i)$ rate term of the desorption of epoxy molecules from the ith adsorption layer to the $(i+1)$th bulk layer (s^{-1})

$\Re_{a,A}$ total adsorption rate of amine species into the i^{th} adsorption layer from the neighboring bulk layers [eq. (8)] (s^{-1})

$\Re_{a,E}$ total adsorption rate of epoxy species into the i^{th} adsorption layer from the neighboring bulk layers [eq. (2)] (s^{-1})

$\Re_{d,A}$ total desorption rate of amine species into the i^{th} adsorption layer from the neighboring bulk layers [eq. (8)] (s^{-1})

$\Re_{d,E}$ total desorption rate of epoxy species into the i^{th} adsorption layer from the neighboring bulk layers [eq. (2)] (s^{-1})

$\Re_{r,A}$ depletion rate of amine species due to the crosslinking chemical reaction [eq. (8)] (s^{-1})

$\Re_{r,E}$ depletion rate of amine species due to the crosslinking chemical reaction [eq. (2)] (s^{-1})

T temperature (K)

T_0 isothermal processing temperature considered in the parametric studies (K)

T_g glass-transition temperature (K)

T_g^0 constant in the DiBenedetto expression in eq. (14) (K)

t time (s)

t' dimensionless time in the parametric study

v volume

v_m molecular volume

X_A molar fraction of PACM20

Greek symbols

α_A $(k_{a,A}/k_{a,E})e^{-(E_{a,A}-E_{a,E}/RT_0)}$, the ratio of the adsorption rates of amine and epoxy molecules

α_f constant in the diffusion coefficient expression in eq. (13) (K^{-1})

β_A $(k_{d,A}/k_{a,E})e^{-(E_{d,A}-E_{a,E}/RT_0)}$, the ratio of the desorption rate of amine molecules to the adsorption rate of epoxy molecules

β_E $(k_{d,E}/k_{a,E})e^{-(E_{d,E}-E_{a,E}/RT_0)}$, the ratio of the desorption rate of epoxy molecules to the adsorption rate of epoxy molecules

δ interphase thickness in terms of molecular layers

δ_0 coordination sphere reaction parameter in the reaction rate expression in eq. (15) (cm^2/s)

δ_A interphase thickness based on the amine concentration profile

δ_E interphase thickness based on the epoxy concentration profile

ΔL physical size of a molecular layer (m)

ϕ_{EA} $(D_{EA}/\Delta L^2 k_{a,E})e^{(E_{a,E}/RT_0)}$, the ratio of the mutual diffusion rate to the adsorption rate of epoxy molecules

Φ_A volume fraction of PACM20

γ $(k_r/k_{a,E})e^{(E_{a,E}/RT_0)}$, adsorption Damköhler number, or the ratio of the chemical reaction rate to the adsorption rate of epoxy molecules

ρ density (kg/m^3)

ρ_A density of PACM20 (kg/m^3)

ρ_E density of DGEBA (kg/m^3)

ε reaction extent, $N_E/N_{E,0}$

References

1. Palmese, G. R. Origin and Influence of Interphase Material Property Gradients in Thermosetting Composites; Technical Report Number 92-25; University of Delaware Center for Composite Materials, Newark, DE 1992.
2. Subramanian, S.; Lesko, J. J.; Reifsnider, K. L.; Stinchcomb, W. W. J Compos Mater 1996, 30, 309.
3. Rydin, R. W.; Varelidis, P. C.; Papaspyrides, C. D.; Karbhari, V. M. J Compos Mater 1997, 31, 182.
4. Drzal, L. T. Adv Polym Sci 1986, 75, 1.
5. Madhukar, M. S.; Drzal, L. T. J Compos Mater 1991, 25, 958.
6. Dong, Z.; Wu, Y. J Mater Sci 1996, 31, 4401.
7. Liu, Y. J.; Xu, N.; Luo, J. F. J Appl Mech 2000, 67, 41.
8. Garton, A.; Stevenson, W. T. K.; Wang, S. Br Polym J 1987, 19, 459.
9. Sellitti, C.; Koenig, J. L.; Ishida, H. Mater Sci Eng A 1990, 126, 235.
10. Hrivnak, J. Interphase Formation in Reacting Systems; Technical Report Number 97-05; University of Delaware Center for Composite Materials, Newark, DE 1997.
11. Scheutjens, J. M. H. M.; Fleer, G. J. J Phys Chem 1979, 83, 1619.
12. Sergeyeva, L. M.; Todosiychuk, T. T.; Fabulyak, F. G. Geterogennye Polim Mater 1974, 79.
13. Ko, Y. S.; Forsman, W. C.; Dziemanowicz, T. S. Polym Eng Sci 1982, 22, 805.
14. Arayasantiparb, D.; McKnight, S.; Libera, M. J Adhes Sci Technol 2001, 15, 1463.
15. Hill, T. L. J Chem Phys 1946, 14, 268.
16. Ponec, V.; Knor, Z.; Cerny, S. Adsorption on Solids; Butterworth: London, 1974.
17. Sanford, W. M. Ph. D. Thesis, University of Delaware, 1987.
18. Press, W. H.; Teukolsky, S. A.; Vetterling, W. T.; Flannery, B. P. Numerical Recipes in FORTRAN; Cambridge University Press; New York, 1986.
19. Mawardi, A.; Pitchumani, R. ASME J Heat Transfer 2003, 125(1), 126.